Structure and Enzymatic Activity of an Intellectual Disability-Associated Ornithine Decarboxylase Variant, G84R

X. Edward Zhou, Chad R. Schultz,[∇] Kelly Suino Powell,[∇] Amy Henrickson, Jared Lamp, Joseph S. Brunzelle, Borries Demeler, Irving E. Vega, André S. Bachmann,* and Karsten Melcher*

ABSTRACT: Ornithine decarboxylase (ODC) is a rate-limiting enzyme for the synthesis of polyamines (PAs). PAs are required for proliferation, and increased ODC activity is associated with cancer and neural over-proliferation. ODC levels and activity are therefore tightly regulated, including through the ODC-specific inhibitor, antizyme AZ1. Recently, ODC G84R has been reported as a partial loss-of-function variant that is associated with intellectual disability and seizures. However, G84 is distant from both the catalytic center and the ODC homodimerization interface. To understand how G84R modulates ODC activity, we have determined the crystal structure of ODC G84R in both the presence and the absence of the cofactor pyridoxal 5-phosphate. The structures show that the replacement of G84 by arginine leads to hydrogen bond formation of R84 with F420, the last residue of the ODC C-terminal helix, a structural element that is involved in the AZ1-mediated proteasomal degradation of ODC. In contrast, the catalytic center is essentially indistinguishable from that of wildtype ODC. We therefore reanalyzed the catalytic activity of ODC G84R and found that it is rescued when the protein is purified in the presence of a reducing agent to mimic the reducing environment of the cytoplasm. This suggests that R84 may exert its neurological effects not through reducing ODC catalytic activity but through misregulation of its AZ1-mediated proteasomal degradation.
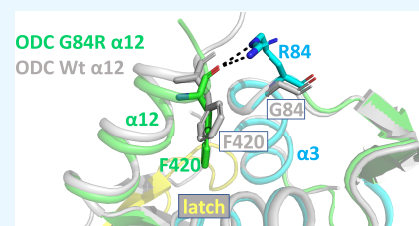
INTRODUCTION

Polyamines (PAs) are multivalent cations that comprise the triamine spermidine and the tetraamine spermine, which are derived from the diamine putrescine. Putrescine is generated by decarboxylation of the amino acid ornithine by the first committed enzyme of polyamine biosynthesis, ornithine decarboxylase (ODC). ODC is a pyridoxal 5-phosphate (PLP)-dependent decarboxylase that is in rapid equilibrium between a catalytically inactive monomeric state and an active dimeric state, both in vitro and in vivo. Homodimerization is required for ODC activity as the two active sites of the dimer are localized at the dimer interface, and each active site is composed of residues from both monomers.[1−3]

PAs are oncometabolites: they are required for cellular proliferation, and their aberrant overaccumulation is associated with many cancers.[4] Their levels are therefore tightly regulated, most notably at the level of ODC. ODC transcription is upregulated by cellular oncogenes, including MYC, while both ODC activity and protein stability are downregulated in response to increased PA levels by at least three dedicated ODC inhibitor proteins called antizymes. At high cellular levels, PAs translationally upregulate antizymes through a translational frame-shifting mechanism.[5] In turn, at elevated levels, antizymes efficiently inhibit the catalytic activity of ODC by binding ODC's dimerization interface, thereby blocking ODC homodimerization and reducing PA levels.[1] Further, binding of the most abundant and most widely expressed antizyme, AZ1, targets ODC for ubiquitin-independent degradation by the 26S proteasome.[6] Release of antizyme inhibition requires another regulatory protein, antizyme inhibitor AzI. AzI is a catalytically inactive ODC paralog that sequesters antizymes by binding them with higher affinity than ODC.[7]

Proteasomal degradation of ODC requires its unstructured C-terminus (residues 424−461),[5,6,8] which has been proposed to mediate the initial insertion of ODC into the proteasome cavity.[9] Consistently, the C-terminus, while required for proteasomal proteolysis, is dispensable for proteasome binding[9] and is structurally unchanged by Az binding as shown by NMR.[10] Rather, Az1 binding breaks interactions between the ODC N-terminus and the C-terminal helix (helix α12) immediately preceding the disordered C-terminus. As a consequence, α12 becomes released into the solvent and more dynamic as it became either completely unresolved[9] or had a strongly increased B-factor[10] in the crystal structures of ODC/AZ1 heterodimers. Both studies therefore concluded that the AZ1-mediated exposure of the C-terminal helix and its

preceding loop induces proteolysis,[9,10] possibly by functioning as a degron, although direct evidence for this function is missing.

ODC G84R is a recently discovered variant that is associated with intellectual disabilities and seizures and that is found in about 0.2% of the overall population and 0.8% among South Asians.[11] Purified, recombinant ODC G84R has been reported to have a 2- to 3-fold lower activity relative to the wildtype protein,[11] yet G84 is distant both to the catalytic site and the dimerization interface. Here, we have determined the crystal structure of ODC G84R(1–423), which revealed that R84 forms hydrogen bonds with the terminal residue of the C-terminal helix, F420. We have further shown that the catalytic activity of purified recombinant ODC G84R is highly sensitive to protein oxidation but largely or fully restored under reducing conditions.

■ MATERIALS AND METHODS

Protein Expression and Purification. Full length ODC and ODC1(1–423) with the mutation G84R were expressed in a pET28 vector with a C-terminal His6 tag. BL21(DE3) cells transformed with this expression plasmid were grown in LB broth at 16 °C to an OD_{600} of ∼1 and induced with 0.1 mM IPTG. The next morning, cells were harvested, resuspended in 150 mL of extract buffer (20 mM Tris [pH 8], 200 mM NaCl, 10% glycerol) per 2 L of cells, and passed three times through a French Press with a pressure set at 1000 Pa. The lysate was centrifuged at 34,571g for 1 h, and the supernatant was loaded on a 5 mL HisTrap FF column (GE Healthcare). The column was washed with 100 mL of buffer A + 25 mM imidazole and eluted with 50 mL of buffer B (20 mM Tris [pH 8], 500 mM imidazole, 10% glycerol). The peak fractions were further purified by passing through at a HiLoad 26/200 Superdex 200 pg column (GE Healthcare) (20 mM Tris [pH 8], 200 mM NaCl, 2 mM DTT, 1 mM EDTA, 10% glycerol). A portion of the eluted protein was complexed with pyridoxal 5′-phosphate monohydrate (PLP) (Sigma-Aldrich) at a five-fold molar excess. The apo and complex proteins were filter-concentrated to 15 mg/mL.

ODC Enzyme Activity Assay. ODC activity was measured using 100 ng of purified ODC protein diluted in a buffer containing 25 mM Tris and 0.1 mM EDTA. Each of the reactions was added to 200 μL of assay mix containing 6.25 mM Tris HCl (pH 7.5), 100 μM L-ornithine, 50 μM pyridoxal-5-phosphate, and 0.1 μCi [1-^{14}C] L-ornithine (American Radiolabeled Chemicals, Inc., specific activity 55 mCi/mmol) +/− 1.56 mM DTT in a microcentrifuge tube. The microcentrifuge tubes were then placed into scintillation vials containing a piece of filter paper saturated with 200 μL of 0.1 M NaOH to capture the release of radiolabeled carbon dioxide. The samples were incubated in a 37 °C incubator while shaking for 30 min. The enzymatic reaction was stopped by adding 250 μL of 5 M sulfuric acid to each sample and incubating at 37 °C while shaking for 30 min. The microcentrifuge tubes were removed from the scintillation vials, and 5 mL of scintillation fluid was added. Disintegrations per minute (DPM) of each sample were measured using a TriCarb liquid scintillation counter (PerkinElmer). The specific ODC activity was expressed as nmol CO2/min/mg protein.

Crystallization. The ODC G84R apo crystals were grown in sitting drop wells with 0.2 μL of protein and 0.2 μL of well solution containing 0.2 M sodium acetate trihydrate pH 7.0, 20% w/v polyethylene glycol 3350. The ODC G84R PLP crystals were also grown in sitting drop wells with 0.2 μL of protein and 0.2 μL of well solution containing 0.2 M sodium acetate trihydrate pH 7.0, 20% w/v polyethylene glycol 3350.

Data Collection, Structure Determination, and Analysis. Both the crystals of apo- and PLP-bound ODC G84R formed in the $P2_12_12_1$ space group. The datasets were collected with an EIGER 16 M pixel array detector at the ID line of sector 21 of the Advanced Photon Source at Argonne National Laboratory (Argonne, IL). The datasets were indexed to 1.85 and 2.35 Å with XD[12] and scaled with AIMLESS in the CCP4 package (http://www.ccp4.ac.uk). The CCP4 program PHASER was used for molecular replacement, with the crystal structure of WT human ODC (PBD code: 7S3F)[13] as a search model. The initial model was manually built in COOT[14] and refined with the PHENIX program phenix.refine.[15] All figures were prepared using PyMOL (DeLano Scientific, San Carlos, CA, http://www.pymol.org).

Analytical Ultracentrifugation (AUC). All AUC experiments were performed at the Canadian Center for Hydrodynamics at the University of Lethbridge, on a Beckman-Coulter Optima AUC. Sedimentation velocity data were collected at 45,000 rpm in an An60Ti rotor, at 20 °C, using standard two-channel epon-charcoal centerpieces with a 1.2 cm pathlength. Data were collected using a UV absorbance detector, scanning in intensity mode. All samples were measured in a buffer containing 10 mM TRIS, pH 7.5, and 100 mM NaCl. Samples measured under reducing conditions had 1 mM TCEP added. All data were analyzed with UltraScan, version 6169.[16] Depending on the sample, 220–280 nm scans were analyzed. To determine if mass action is present, multiple loading concentrations spanning a significant concentration range, centered around the Kd, should be examined. Three different concentrations spanning approximately a 20-fold concentration range for ODC WT and ODC G84R were measured by AUC without a reductant and one concentration for ODC WT and ODC G84R with a reductant present (see Table S1). Molar extinction coefficients were determined by fitting absorbance spectra, taken between 210 and 310 nm, of three different concentrations from each sample to a global extinction spectrum using the spectrum fitter in UltraScan, and subsequently scaling the resulting profile with the molar extinction coefficient with the value at 280 nm derived from sequence by UltraScan. Molar extinction coefficient profile fits are shown in Figure S1 (ODC WT) and Figure S2 (ODC G84R) and in table format for both ODC versions (Tables S2 and S3 for the wildtype and mutant, respectively). The partial specific volume of ODC was determined from sequence with UltraScan and found to be 0.732 mL/g.

AUC Data Analysis. Sedimentation and diffusion transport in the ultracentrifugation cell were described by the Lamm equation, which can be solved using adaptive finite element methods.[17,18] Whole boundary data obtained in SV experiments were fitted by linear combinations of finite element solutions using advanced optimization routines[19−21] that are typically implemented on a supercomputer.[22] For this study, all SV data were initially fitted with the two-dimensional spectrum analysis,[19] with simultaneous time- and radially invariant noise subtraction, and fitting of boundary conditions. SV experiments were then evaluated by the enhanced van Holde−Weischet method.[23] Two-dimensional spectrum analysis results were refined by the genetic algorithm method.[20]

Confidence intervals (95%) were obtained with the Monte Carlo analysis.[21] Partial concentrations were obtained in optical density units and converted to molar concentrations using the determined molar extinction coefficients at 225 nm and taking the pathlengths of the AUC cell (1.2 cm) into account.

Mass Spectrometry (MS). *Sample Preparation.* One of the purified WT (3 μg) and one of the purified ODC G84R proteins that were used for activity measurement were buffer-exchanged (300 μL 50 mM ammonium bicarbonate, pH 8.0) using a 3 kDa spin filter (Amicon) at 18,000*g* for 30 min at 4 °C. After exchange, the samples were dried to completion at 30 °C (∼2 h) and resuspended in 50 μL of digestion buffer (25 mM ammonium bicarbonate, pH 8.0, 50% acetonitrile). Trypsin and Lys-C (Promega) were added at 1:10 (w/w trypsin:protein) and 1:20 (w/w lys-C:protein) ratios for protein digestion over 17 h at 37 °C. After digestion, samples were dried to completion at 30 °C (∼2 h) and resuspended in 50 μL of analysis buffer (2% acetonitrile, 0.1% formic acid).

Liquid Chromatography and Bottom-Up Mass Spectrometry. Peptides were separated and analyzed by nano LC−MS/MS. Each sample (300 ng) was injected using an Ultimate 3000 autosampler (Dionex, ThermoFisher). Peptides were trapped on an Acclaim PepMap C18 trapping column (ThermoFisher) at 5 μL/min in buffer containing 2% acetonitrile and 0.1% formic acid. After a 5 min desalting period, peptides were separated using linear gradients at 350 nL/min on a C18 EASY-Spray column (2 μm particle size, 75 μm × 250 mm) (ThermoFisher). The gradients used were, in order, 4−40% solvent B over 5−100 min, 40−65% solvent B over 100−102 min, 65−95% solvent B over 102−105 min, 95% solvent B over 105−116 min, and 95−4% solvent B over 116−117 min (gradient solvent A contained 0.1% formic acid, and solvent B contained acetonitrile and 0.1% formic acid). The liquid chromatography eluate was interfaced to a Q Exactive HF-X (ThermoFisher) via an EASY-Spray ionization source with an electrospray voltage of 1.9 kV at a 2.0 mm tip to an inlet distance. The ion capillary temperature was 280 °C, and the RF level was 55.0.

MS1 scans of *m/z* 300−1500 were acquired in the orbitrap with a resolution ($M/\Delta M$) of 60,000 at 200 *m/z*, maximum injection time of 45 ms, and automatic gain control (AGC) target of 3×10^6. The top 20 MS2 scans were acquired in the orbitrap with a resolution ($M/\Delta M$) of 30,000 at 200 *m/z*, maximum injection time of 54 ms, AGC target of 1×10^5, and isolation width of 1.3 *m/z*. HCD fragmentation was NCE 28, dynamic exclusion was 30 s, and singly charged and greater than +6 charged ions were excluded from selection.

Data Analysis. Mass spectra were identified against databases containing the digestion enzymes and either WT or ODC G84R sequences (Acc: P11926), using Proteome Discoverer (v. 2.2.0.388, 2017). Parameters were set as follows: at least two peptides (minimum length = 6, minimum precursor mass = 350 Da, maximum precursor mass = 5000 Da), tolerance of 10 ppm for precursor ions and 0.02 Da for fragment ions (b and y ions only), and Percolator FDR (strict minimum value 0.01). Dynamic modifications included methionine oxidation (+15.995 Da), cysteine glutathionylation (+305.068 Da), cysteine sulfenylation (+15.995 Da), cysteine sulfinic acid (+31.990 Da), and cysteine sulfonic acid (+47.985 Da).

Peptide retention times, MS1 area measurements, and peptide ratio calculations were performed by Skyline (version

4.2.0). All peaks were manually corrected by comparing selected retention times against those reported by Proteome Discoverer and ensuring idotp values greater than 0.90. The precursor [M], [M + 1], and [M + 2] isotopic peaks from the two most intense peptide charge states were used for peak area summation. MS1 mass tolerance matched the acquisition method (60,000 resolution at 200 *m/z*).

■ RESULTS

Structure of ODC G84R. The ODC G84R mutation is associated with intellectual disabilities and seizures, and the G84R protein has reduced catalytic activity in an in vitro assay.[11] To gain mechanistic insight into the mutant phenotype, we purified recombinant, human His6-ODC1(1-423) G84R and determined its crystal structure both in the presence and in the absence of the ODC cofactor pyridoxal 5′-phosphate (PLP) at resolutions of 1.85 and 2.35 Å, respectively (Table 1). ODC1(1-423) lacks the unstructured

**Table 1. Data Collection and Structure Refinement Statistics**

	ODC1 G84R apo	ODC1 G84R/PLP
PDB entry	7U6P	7U6U
data collection		
space group	$P2_12_12_1$	$P2_12_12_1$
cell dimensions		
a, b, c (Å)	74.81, 85.88, 154.74	74.15, 86.10, 153.28
α, β, γ (°)	90, 90, 90	90, 90, 90
no. reflections		
total	353,747 (34,917)	578,271 (30,677)
unique	42,293 (4104)	84,340 (4377)
resolution (Å)	45.6−2.35 (2.43−2.35)[a]	45.3−1.85 (1.88−1.85)[a]
R_{sym} or R_{merge}	0.196 (1.35)	0.135 (1.529)
$I/\sigma I$	9.4 (4.4)	11.4 (2.5)
$CC_{1/2}$	0.993 (0.867)	0.996 (0.617)
completeness (%)	99.9 (99.9)	99.9 (99.8)
redundancy	8.4 (8.5)	6.9 (7.0)
refinement		
resolution (Å)	49−1.82 (1.84−1.82)	49−1.85 (1.84−1.82)
no. reflections	90,252 (2778)	90,252 (2778)
R_{work}/R_{free}	18.82/22.45 (23.6/29.5)	18.06/20.36 (25.3/28.2)
no. atoms/residues		
protein	6701/815	6899/806
ligand/ion	2	2
water	305	553
B-factors		
protein	37.7	27.5
ligand/ion	35.1	22.3
water	38.8	37.3
r.m.s. deviations		
bond lengths (Å)	0.004	0.006
bond angles (°)	0.653	0.848
Ramachandran plot (%)		
favored	97.39	98.11
outliers	0	0
MolProbity score	1.40	1.18

[a]Values in parentheses are for the highest-resolution shell.
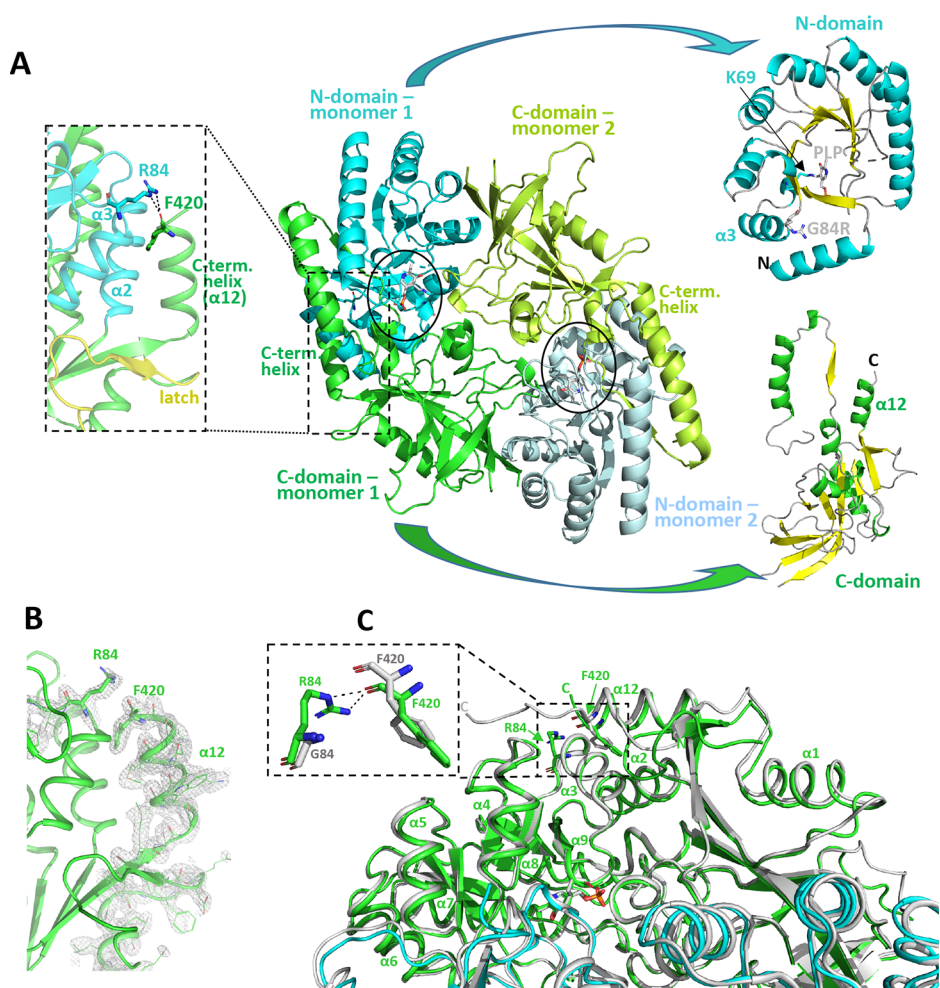
Figure 1. ODC G84R crystal structure. (A) ODC G84R homodimer in the presence of PLP. The N- and C-domains of one monomer are shown in cyan and green, respectively, and of the other monomer in light cyan and light green, respectively, with the catalytic centers indicated by black ovals. The inset on the left is a close-up of the G84R region with R84 and F420 shown in stick representation and the two hydrogen bonds between them shown as dashed lines. Right side: cartoon structures of the isolated N-domain (cyan: α-helices, yellow: β-strands) and isolated C-domain (green: α-helices, yellow: β-strands). (B) 2mFo-DFc electron density map of R84 and helix α12 with F420 and the preceding loop contoured at 1 σ. Side chains other than R84 and F420 are shown in line representation. (C) Structure overlay of ODC G84R (cyan and green) with wildtype ODC (PDB 1D7K, gray). G/R84, F420, and PLP are shown in stick representation.
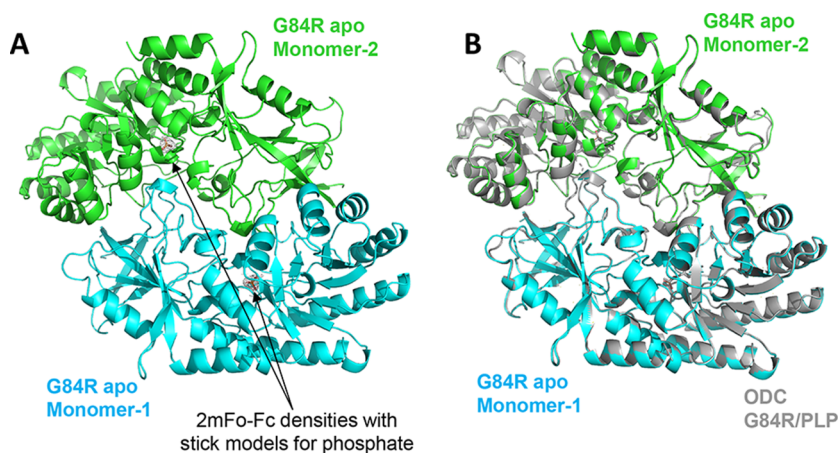
Figure 2. Structure of PLP-free ODC G84R. (A) Overview of human ODC G84R in the absence of added PLP. The arrows point to the 2mFo-Fc density in the ODC-binding pocket of each monomer, contoured at 1 σ. The color code is the same as in Figure 1. The stick model for phosphate was built into the density. (B) Structure of human ODC G84R in the absence of PLP (cyan and green) overlaid with the structure of human ODC G84R/PLP (gray).
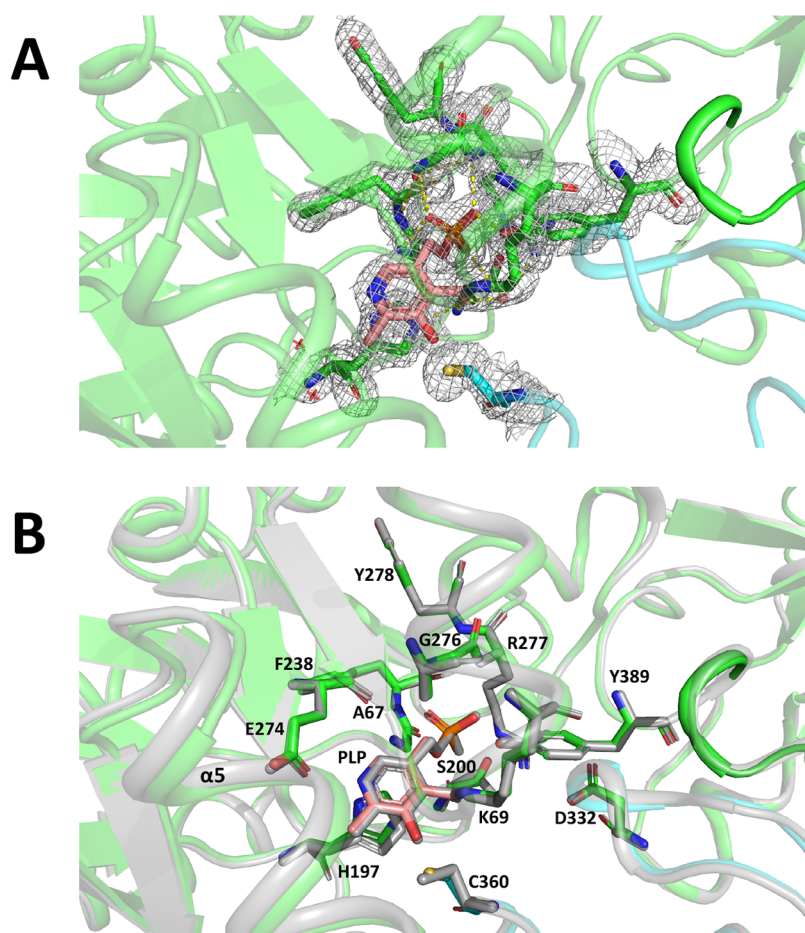
Figure 3. G84R does not change the conformation of the ODC catalytic center. (A) ODC G84R catalytic center. The two monomers are shown in green and cyan, and PLP is shown in pink. PLP and pocket residues are shown in stick representation and are overlaid with the 2mFo-Fc map contoured at 1 σ. (B) Structural alignment of the catalytic centers of ODC G84R (color) and wildtype ODC (gray; PDB 1D7K) with PLP and pocket residues shown in stick representation. Helix $\alpha 5$ is on the surface of ODC distant from the catalytic center and forms part of the AZ1-binding site.

C-terminal 38 amino acids of ODC, which are not required for catalytic activity.[24] The structures show the characteristic ODC dimer fold, in which the two catalytic centers of the dimer are localized at the dimer interface, and in which each catalytic center is formed by residues from both monomers (Figures 1 and 2), as previously described.[25] Each monomer consists of an N-terminal triosephosphate isomerase (TIM) α/β barrel and a C-terminal mixed β-sheet surrounded by helices (right-side insets in Figure 1A). The structure of the PLP-containing G84R mutant protein is very similar to the previously determined structure of human wildtype ODC (PDB 1D7K) with an RMSD value of 0.857 Å (Figure 1C) and to the structure of ODC G84R in the absence of PLP (RMSD = 0.548 Å; Figure 2). Interestingly, the 2mFo-Fc density indicated that in the absence of added PLP, the PLP pocket was occupied by a phosphate group that stabilizes the catalytic center and the dimer interface similar to the cofactor PLP.

Exchange of Gly84 against arginine in helix $\alpha 3$ allowed formation of two hydrogen bonds between the guanidium group of $\alpha 3$-R84 and the carbonyl group of $\alpha 12$-F420 (Figure 1A, left-side inset, and Figure 1B,C). Importantly, these strong hydrogen bonds anchor the dynamic C-terminal helix ($\alpha 12$) to the end of the stable helix $\alpha 3$. While the position of $\alpha 3$ was unaltered in the mutant protein, the C-terminus of $\alpha 12$ was
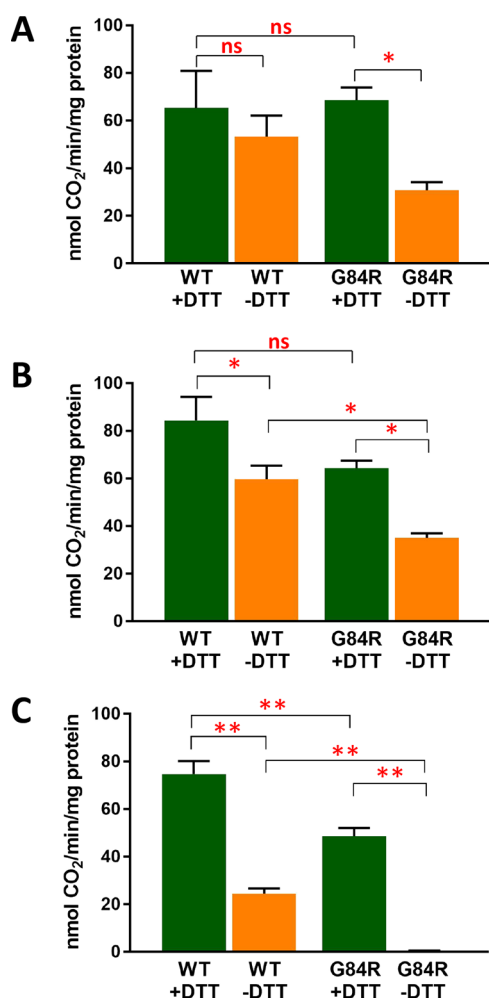
repositioned by 1.7 Å closer to the guanidium group of R84 (Figure 1C).

An alternative, modeled bond formation was proposed between the guanidium group of R84 and the carboxyl group of D424,[11] which directly follows the C-terminal helix and is the first amino acid of the unstructured C-terminus that is missing in our ODC construct.

In addition to the change in the C-terminus of ODC, we observed small displacements of peripheral loops and helices in the structure of ODC G84R (Figure 1C). In contrast, the catalytic center is almost identical between wildtype and G84R ODC (Figure 3B). The catalytic center is formed by PLP, which in the absence of a substrate is covalently bound to ODC K69, and the residues surrounding the PLP-K69 adduct.

ODC1 G84R is Catalytically Active. The previously reported activities of wildtype and G84R ODC were determined from preparations generated by Ray Biotech.[11] We reanalyzed ODC activity using both the constructs lacking the unstructured C-terminus and full-length His6-tagged human wildtype and G84R ODC. These four proteins were expressed in *Escherichia coli* and purified by sequential Ni-affinity and size exclusion chromatography, using the same conditions as for the ODC(1-423) G84R protein that we had used for crystallization. To our surprise, we found that our ODC G84R protein preparation had an as high [ODC(1-

423)] (Figure 4A) or only mildly lower [full length ODC] (Figure 4B) activity than the wildtype protein. This result

Figure 4. Activities of ODC wildtype (WT) and ODC G84R preparations in the absence and presence of DTT in the storage buffer. (A, B) Truncated (A) and full length (B) ODC prepared for this study by two-step chromatography with 2 mM DTT in size exclusion chromatography and storage buffers. (C) ODC prepared by Ray Biotech by one-step chromatography in the absence of DTT; +/−DTT: the presence/absence of 1.56 mM DTT in the ODC assay buffer. Data are from two (A, B) or three (C) independent experiments, each repeated three times (n = 6 or 9). Error bars indicate SEM. One-way analysis of variance (ANOVA): *P < 0.05, **P < 0.0001.

differed from the one using proteins generated by Ray Biotech, which showed a 2- to 3-fold lower catalytic activity for ODC G84R[11] and was therefore implying that the G84R mutation confers a loss of function. We confirmed that the Ray Biotech ODC G84R preparation has a reduced catalytic activity, although the level of reduction was lower than previously reported (∼63% of activity left as opposed to ∼40%) (Figure 4C).

The Ray Biotech preparation differed from our preparations by having been purified only by a single Ni-affinity chromatography step and by the lack of a reducing agent in the ODC storage buffer. ODC has 12 potentially oxidizable cysteines per monomer, including the catalytic cysteine C360, and its activity may therefore be sensitive to oxidation. To test whether the mutant protein is more sensitive to oxidative conditions than the wildtype protein, we removed the reductant dithiothreitol (DTT) from the assay buffer. For our ODC preparations, which contain DTT in the storage buffer, the absence of DTT from the assay buffer did not affect the activity of wildtype ODC but reduced the activity of the mutant protein about 2-fold (Figure 4A,B). In the case of the Ray Biotech protein preparation, which lacks DTT in the storage buffer, removal of DTT from the assay buffer reduced the activity of the wildtype protein about 3-fold and led to a complete loss of the activity of the mutant protein (Figure 4C). Together, this suggested that ODC G84R is active under reducing conditions but is more sensitive to experimentally induced oxidative conditions.

ODC G84R Aggregates in the Absence of Reductants. ODC is in a dynamic monomer−dimer equilibrium, with the homodimer form being required for catalytic activity. We used analytical ultracentrifugation (AUC) sedimentation velocity (SV) experiments to quantitate the monomer−dimer equilibrium of human wildtype ODC and ODC G84R in the absence and presence of the reducing agent tris(2-carboxyethyl)phosphine (TCEP; DTT is not compatible with AUC). SV experiments provide a clear distinction between homogeneous preparations,[26] the presence of aggregates,[27] and reversible self-association[28,29] in response to mass action.

As shown in Figure 5A, both wildtype and mutant ODC undergo a monomer to dimer shift with increasing concentrations. Two of the ODC G84R samples showed evidence of irreversible aggregation and formation of higher order oligomers but only in the absence of TCEP (Figure 5A). While we observed that the mutant is prone to aggregation under oxidizing conditions, in the presence of 1 mM TCEP, and at concentrations above the reported Kd,[30] the sedimentation behaviors of wildtype and G84R ODC are

Table 2. Hydrodynamic Parameters Derived from the Genetic Algorithm-Monte Carlo Analysis[a]

sample	sedimentation coefficient (s, 10^{-13})	diffusion coefficient (cm^2/s, 10^{-7})	molar mass (kDa)	frictional ratio
		ODC wildtype		
monomer	4.57 (4.53, 4.61)	7.35 (7.23, 7.47)	56.3 (55.3, 57.2)	1.15 (1.14, 1.16)
dimer	5.66 (5.65, 5.68)	4.31 (4.21, 4.41)	118.9 (116.2, 121.8)	1.53 (1.51, 1.55)
		ODC G84R		
monomer	3.84 (3.82, 3.86)	7.61 (7.48, 7.74)	48.6 (47.8, 49.4)	1.15 (1.11, 1.18)
dimer	5.60 (4.83, 6.36)	4.94 (4.29, 5.59)	123.2 (117.5, 128.9)	1.60 (1.55, 1.64)

[a]Values in parentheses are 95% confidence intervals derived from the Monte Carlo analysis. Molar masses are estimates based on a sequence-derived partial specific volume and are in good agreement with molar masses calculated from sequence (51.2 kDa); any discrepancies indicate a variation in the partial specific volume between the monomer and dimer.
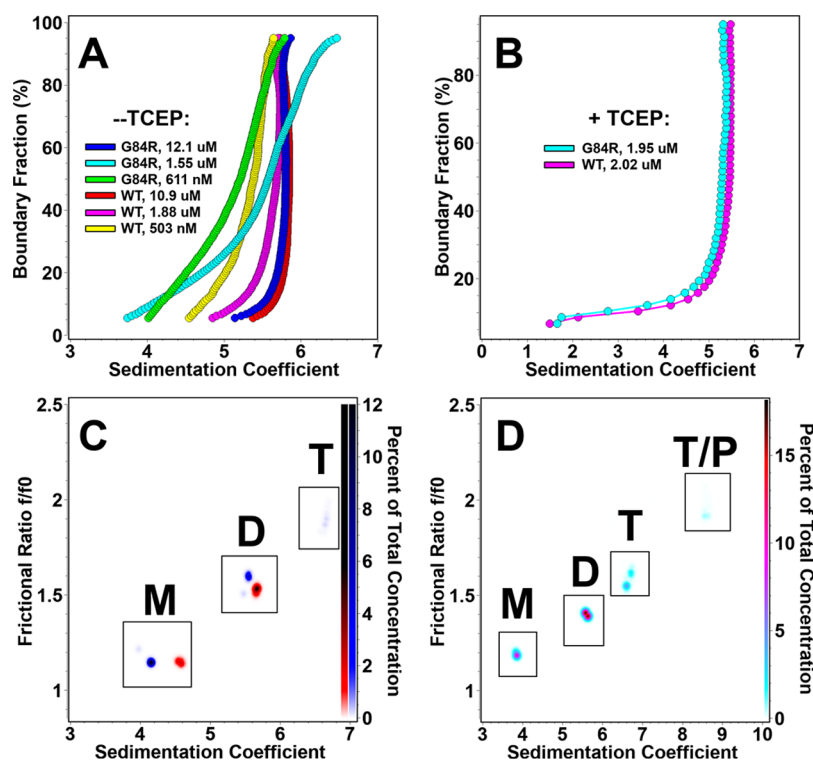
Figure 5. Sedimentation velocity analysis of ODC wildtype (WT) and ODC G84R. (A) Van Holde−Weischet integral distribution plots of ODC WT at 10.87 μM (red), 1.88 μM (magenta), and 503 nM (yellow) and ODC G84R at 12.1 μM (blue), 1.55 μM (cyan), and 611 nM (green), in the absence of TCEP. All distributions show mass action induced shifts of the sedimentation coefficient and a characteristic monomer−dimer distribution shape. For the 1.55 μM ODC G84R sample, and to a lesser degree the 611 nM ODC G84R sample, the distribution also shows evidence of irreversible aggregation when TCEP is not added. (B) Van Holde−Weischet integral distribution plots of ODC WT at 2.02 μM (magenta) and ODC G84R at 1.95 μM (cyan) in the presence of 1 mM TCEP, showing nearly identical sedimentation coefficient distribution with the majority of the signal consistent with a dimer. The lower s-value portion of the distribution reflects the partial contribution of TCEP, which is a small, slow sedimenting molecule that absorbs at 230 nm and thus precludes accurate Kd determination in the presence of TCEP. (C) Genetic algorithm-Monte Carlo analysis of the 503 nM ODC WT (red) and the 611 nM ODC G84R sample (blue). Monomer (M), dimer (D), and trimer (T) species are indicated in the labeled boxes. Only the ODC G84R sample shows slight evidence of the irreversible trimer. (D) Genetic algorithm-Monte Carlo analysis of the 1.55 μM ODC G84R sample. While the monomer (M) and dimer (D) are the predominant species, clear evidence is seen for the presence of irreversible aggregates with sizes that are consistent with the trimer (T) and tetramer or pentamer (P/T). In all cases, it is evident that higher order oligomers, irreversible or not, are increasingly anisotropic. For panels (C, D), the partial concentration of each species is indicated by the color density (right axis); additional details are shown in Table 2.

very similar, and no aggregation is observed for the mutant (Figure 5B). This suggests that the aggregation of ODC G84R is responsible for the reduced catalytic activity of ODC G84R in the absence of a reducing agent. Further examination of aggregated ODC G84R velocity data using genetic algorithm-Monte Carlo analysis shows that in the absence of TCEP, the mutant protein forms higher order oligomers, which exhibit increased anisotropies with an increased oligomerization state, suggesting that ODC G84R is prone to the formation of intermolecular disulfide bonds (compare Figure 5C and Figure 5D). Finally, we used mass spectrometry to identify mutant-specific amino acid oxidative modifications of cysteine residues by glutathionylation, sulfenylation, and the formation of sulfinic acid or sulfonic acid (Tables 3 and 4). Mass spectrometry also identified two main pairs of intermolecular disulfide bonds: C11-C11 and C360-C360 (Table 5), consistent with the formation of higher order ODC complexes observed by the AUC SV experiments in the absence of TCEP.

Since C360 is required for ODC catalytic activity, C360-C360 disulfide bond formation might also explain the reduced catalytic activity of ODC in the absence of reducing agents, especially for the mutant protein. While this experiment cannot confidently evaluate the relative frequencies of oxidative modifications of wildtype versus ODC G84R, none of the resolved peptides showed mutant-specific increases in oxidized/unoxidized peptides ratios nor disulfide bound/unbound peptides ratios for C11-C11 or C360-C360. Therefore, a modification in an unresolved peptide might be responsible for the mutant-specific oxidation sensitivity. Together, the results are most consistent with the oxidation sensitivity of ODC G84R being due to its propensity to form disulfide-linked aggregates.

■ DISCUSSION

ODC gain-of-function mutations have been associated with hyper-proliferative diseases, including cancer, infections, overgrowth, neural overproliferation,[31] and the ODC-linked neurodevelopmental disorder, Bachmann−Bupp syndrome.[32−34] Recently, Prokop et al. have identified ODC G84R as a variant associated with intellectual disability and seizures. Activity assays using recombinant ODC indicated that G84R is a loss-of-function mutation, and the authors hypothesized that ODC partial loss-of-function may lead to neural depletion.[11] To gain more mechanistic insight, we determined the crystal structure of ODC G84R and biochemi-

Table 3. ODC Peptide Identifications and Number of ODC Peptide Spectral Matches (PSM) for Each Oxidation State[a]

Annotated Sequence	Position in Protein	C/M Oxidations	WT PSMs	G84R PSMs
[-].MNNFGN-EEFDCHFLDEGFTAKDILDQKINEVSSSDDK.[D]	1-37	4	1	
[-].MNNFGN-EEFDCHFLDEGFTAKDILDQKINEVSSSDDK.[D]	1-37	3	1	
[-].MNNFGNEEFDCHFLDEGFTAKDILDQK.[I]	1-27	3	2	3
[-].MNNFGNEEFDCHFLDEGFTAKDILDQK.[I]	1-27	4	3	1
[-].MNNFGNEEFDCHFLDEGFTAKDILDQK.[I]	1-27	0	1	
[-].MNNFGNEEFDCHFLDEGFTAKDILDQK.[I]	1-27	2	2	1
[-].MNNFGNEEFDCHFLDEGFTAK.[D]	1-21	4	6	8
[-].MNNFGNEEFDCHFLDEGFTAK.[D]	1-21	3	9	6
[-].MNNFGNEEFDCHFLDEGFTAK.[D]	1-21	2	1	5
[-].MNNFGNEEFDCHFLDEGFTAK.[D]	1-21	1	1	1
[-].MNNFGNEEFDCHFLDEGFTAK.[D]	1-21	0	6	2
[K].DILDQKINEVSSSDDKDAFYVADLGDILK.[K]	22-50	0	4	4
[K].DILDQKINEVSSSDDK.[D]	22-37	0	2	3
[K].DILDQK.[I]	22-27	0	4	4
[K].INEVSSSDDKDAFYVADLGDILKK.[H]	28-51	0	26	32
[K].INEVSSSDDKDAFYVADLGDILK.[K]	28-50	0	3	4
[K].DAFYVADLGDILKK.[H]	38-51	0	12	9
[K].DAFYVADLGDILK.[K]	38-50	0	5	5
[R].VTPFYAVKCNDSKAIVK.[T]	62-78	3	1	1
[R].VTPFYAVKCNDSKAIVK.[T]	62-78	2		2
[R].VTPFYAVKCNDSK.[A]	62-74	3	2	1
[R].VTPFYAVKCNDSK.[A]	62-74	2	2	2
[R].VTPFYAVK.[C]	62-69	0	43	44
[K].TLAATGTGFDCASKTEIQLVQSLGVPPER.[I]	79-107	1	1	
[K].TLAATGTGFDCASKTEIQLVQSLGVPPER.[I]	79-107	0	3	
[K].TLAATGTGFDCASKTEIQLVQSLGVPPER.[I]	79-107	2	4	
[K].TLAATGTGFDCASKTEIQLVQSLGVPPER.[I]	79-107	3	5	
[K].TLAATGTGFDCASK.[T]	79-92	2	2	
[K].TLAATGTGFDCASK.[T]	79-92	3	3	
[K].TLAATGTGFDCASK.[T]	79-92	0	4	
[R].TGFDCASKTEIQLVQSLGVPPER.[I]	85-107	0		10
[R].TGFDCASKTEIQLVQSLGVPPER.[I]	85-107	2		4
[R].TGFDCASKTEIQLVQSLGVPPER.[I]	85-107	3		4
[K].TEIQLVQSLGVPPER.[I]	93-107	0	42	39
[R].IIYANPCKQVSQIK.[Y]	108-121	0	1	1

Annotated Sequence	Position in Protein	C/M Oxidations	WT PSMs	G84R PSMs
[R].IIYANPCKQVSQIK.[Y]	108-121	2		1
[R].IIYANPCKQVSQIK.[Y]	108-121	3	2	2
[R].IIYANPCK.[Q]	108-115	2	1	1
[R].IIYANPCK.[Q]	108-115	3	2	2
[K].QVSQIKYAANNGVQMMTFDSEVELMK.[V]	116-141	1		2
[K].QVSQIKYAANNGVQMMTFDSEVELMK.[V]	116-141	0		2
[K].YAANNGVQMMTFDSEVELMKVAR.[A]	122-144	0	1	
[K].YAANNGVQMMTFDSEVELMK.[V]	122-141	0	1	
[K].AKLVLR.[I]	149-154	0	1	1
[R].IATDDSKAVCRLSVK.[F]	155-169	3	1	1
[R].IATDDSKAVCRLSVK.[F]	155-169	2		1
[K].FGATLR.[T]	170-175	0	22	18
[R].AKELNIDVVGVSFHVGSGCTDPETFVQAIS-DAR.[C]	184-216	2		2
[R].AKELNIDVVGVSFHVGSGCTDPETFVQAIS-DAR.[C]	184-216	3		1
[K].ELNIDVVGVSFHVGSGCTDPETFVQAISDAR.[C]	186-216	2		1
[R].CVFDMGAEVGFSMYLLDIGGGFPGS-EDVKLK.[F]	217-247	4	1	1
[R].CVFDMGAEVGFSMYLLDIGGGFPGSEDVK.[L]	217-245	4	1	1
[K].LKFEEITGVINPALDK.[Y]	246-261	0	8	8
[K].FEEITGVINPALDKYFPSDSGVR.[I]	248-270	0	38	40
[K].FEEITGVINPALDK.[Y]	248-261	0	17	19
[K].YFPSDSGVR.[I]	262-270	0	22	17
[R].IIAEPGRYYVASAFTLAVNIIAKK.[I]	271-294	0	5	10
[R].IIAEPGRYYVASAFTLAVNIIAK.[K]	271-293	0	27	43
[R].IIAEPGR.[Y]	271-277	0	2	1
[R].YYVASAFTLAVNIIAKK.[I]	278-294	0	5	4
[R].YYVASAFTLAVNIIAK.[K]	278-293	0	7	1
[K].RPKPDEKYYSSSIWGPTCDGLDRIVER.[C]	343-369	0	2	1
[K].RPKPDEKYYSSSIWGPTCDGLDRIVER.[C]	343-369	2		1
[K].RPKPDEKYYSSSIWGPTCDGLDRIVER.[C]	343-369	3	4	1
[K].RPKPDEKYYSSSIWGPTCDGLDR.[I]	343-365	0	4	2
[K].RPKPDEKYYSSSIWGPTCDGLDR.[I]	343-365	2	2	1
[K].RPKPDEKYYSSSIWGPTCDGLDR.[I]	343-365	3	5	3
[K].YYSSSIWGPTCDGLDRIVER.[C]	350-369	3	2	3
[K].YYSSSIWGPTCDGLDR.[I]	350-365	0	1	1
[K].YYSSSIWGPTCDGLDR.[I]	350-365	2	1	1
[K].YYSSSIWGPTCDGLDR.[I]	350-365	3	4	3

[a]The data shown are from one of the two WT and one of the two G84R ODC preparations that were analyzed in Figure 4B. Shown are all MS-identified cysteine-containing ODC peptides. Oxidations: number of oxygen incorporations (1: cysteine S-sulfenylation [Cys-SOH], 2: cysteine-sulfinic acid [Cys-SO₂H], 3: cysteine sulfonic acid [Cys-SO₃H], 4: cysteine sulfonic acid + methionine oxidation). Glutathionylation was not detected. Peptides that are specific to the WT (orange) or G84R (green) form have the same color background. WT: wildtype ODC, G84R: mutant ODC.

cally and biophysically analyzed purified wildtype and mutant ODC.

Our crystal structures of ODC(1-423) G84R demonstrated that the mutant residue, R84, localized on helix α3, can form hydrogen bonds with the last residue of the dynamic ODC C-terminal helix, α12, independent of the presence or absence of the catalytic cofactor PLP. The mutant protein also differed from wildtype ODC by small displacements of peripheral loops and helices, yet the catalytic centers of wildtype and mutant protein were largely superimposable. We further demonstrated that the catalytic activity of purified, recombinant ODC G84R is highly sensitive to oxidizing conditions, i.e., the absence of reducing agents such as DTT or TCEP, which prevent oxidation from air. However, through cellular reductants such as glutathione and the disulfide bond-resolving protein thioredoxin, the cytoplasm is a reducing environment. When

we purified and stored ODC G84R in the presence of low concentrations of the reductant DTT, the protein had only mildly, statistically insignificant, lower activity than wildtype ODC. As shown by sedimentation velocity analysis, ODC G84R, in contrast to wildtype ODC, is prone to oxidation-induced aggregation, which we suggest is mediated through intermolecular disulfide bond formation. However, the molecular basis of the oxidation sensitivity of the mutant protein is not obvious from our crystal structures because we determined the structures in the presence of 2 mM DTT, and our attempts to crystallize ODC G84R in the absence of a reducing agent were unsuccessful.

Since recombinant ODC G84R remained catalytically active under relatively mildly reducing conditions, we speculate that its association with pathological phenotypes might be due to the misregulation of its AZ1-mediated proteasomal degrada-

Table 4. ODC Oxidized to Unoxidized Ratio Comparison[a]

Peptide	Oxidations	ODC WT Oxidized Area / ODC WT Unoxidized Area	ODC G84R Oxidized Area / ODC G84R Unoxidized Area	G84R Ratio / WT Ratio
MNNFGNEEFDCHFLDEGFTAK	1	0.128	0.142	1.109
	2	5.907	4.621	0.782
	3	5.427	4.265	0.786
	4	1.524	1.209	0.793
MNNFGNEEFDCHFLDEGFTAKDILDQK	2	2.201	1.989	0.904
	3	1.988	1.771	0.891
	4	0.543	0.467	0.859
VTPFYAVKCNDSK	2	0.005	0.005	0.953
	3	0.011	0.011	0.995
IIYANPCK	2	0.918	0.716	0.780
	3	2.826	2.264	0.801
IIYANPCKQVSQIK	2	0.153	0.130	0.849
	3	5.238	4.390	0.838
RPKPDEKYYSSSIWGPTCDGLDR	2	1.366	1.195	0.875
	3	2.014	1.729	0.859
YYSSSIWGPTCDGLDR	2	1.045	1.132	1.083
	3	1.889	1.935	1.024
YYSSSIWGPTCDGLDRIVER	2	0.455	0.631	1.387
	3	0.191	0.243	1.274

[a]Peptides that differ only by missed cleavages have the same color background.

Table 5. ODC Intermolecular Disulfide Bond Formation

disulfide bond	peptide	ODC WT bonded area/ODC WT unbonded area	ODC G84R bonded area/ODC G84R unbonded area	G84R ratio/WT ratio
C11-C11	MNNFGNEEFDCHFLDEGFTAK	1.079457521	0.906684697	0.840
C36-C360	YYSSSIWGPTCDGLDR	4.813072205	3.638568163	0.756

tion rather than due to compromised catalytic activity. Both the structure of ODC(1-423) and the modeled structure of full length ODC reported previously[11] show that R84 interacts with, and likely stabilizes, the border between the C-terminal helix and the unstructured C-tail of ODC, whose dynamics are required for Az1-mediated ODC degradation. We hypothesize that their stabilization increases cellular ODC levels and thereby total ODC activity as well as polyamine levels. Future investigation will be needed to understand the cellular regulation of ODC G84R in a physiological context.

■ ASSOCIATED CONTENT

ⓢ Supporting Information

The Supporting Information is available free of charge at https://pubs.acs.org/doi/10.1021/acsomega.2c04702.

ODC WT and ODC G84R absorbance profile, molar extinction coefficient profile, and AUC loading concentrations (two supplemental figures and three supplemental tables) (PDF)

■ AUTHOR INFORMATION

Corresponding Authors

André S. Bachmann − *Department of Pediatrics and Human Development, College of Human Medicine, Michigan State University, Grand Rapids, Michigan 49546, United States;* ⓞ orcid.org/0000-0002-6510-8560; Email: bachma26@msu.edu

Karsten Melcher − *Department of Structural Biology, Van Andel Institute, Grand Rapids, Michigan 49503, United States;* ⓞ orcid.org/0000-0002-9125-4027; Email: melcher.karsten@yahoo.org

Authors

X. Edward Zhou − *Department of Structural Biology, Van Andel Institute, Grand Rapids, Michigan 49503, United States*

Chad R. Schultz − *Department of Pediatrics and Human Development, College of Human Medicine, Michigan State University, Grand Rapids, Michigan 49546, United States*

Kelly Suino Powell − *Department of Structural Biology, Van Andel Institute, Grand Rapids, Michigan 49503, United States*

Amy Henrickson − *Department of Chemistry and Biochemistry, The University of Lethbridge, Lethbridge, AB T1K3M4, Canada;* ⓞ orcid.org/0000-0003-3266-5202

Jared Lamp − *Department of Translational Neuroscience, Integrated Mass Spectrometry Unit, College of Human Medicine, Michigan State University, Grand Rapids,*

Michigan 49503, United States; ⊙ orcid.org/0000-0002-7187-7657

Joseph S. Brunzelle − *Northwestern University Synchrotron Research Center, Life Sciences Collaborative Access Team, Northwestern University, Argonne, Illinois 60439, United States*

Borries Demeler − *Department of Chemistry and Biochemistry, The University of Lethbridge, Lethbridge, AB T1K3M4, Canada; Department of Chemistry and Biochemistry, The University of Montana, Missoula, Montana 59812, United States;* ⊙ orcid.org/0000-0002-2414-9518

Irving E. Vega − *Department of Translational Neuroscience, Integrated Mass Spectrometry Unit, College of Human Medicine, Michigan State University, Grand Rapids, Michigan 49503, United States*

Complete contact information is available at:
https://pubs.acs.org/10.1021/acsomega.2c04702

Author Contributions

[∇]C.R.S. and K.S.P. contributed equally to this work. A.S.B. and K.M. conceived the project. X.E.Z., B.D., I.E.V., A.S.B., and K.M. designed the experiments. X.E.Z., C.R.S., K.S.P., A.H., J.L., and J.S.B. performed and/or interpreted the experiments; K.M. wrote the paper with support from all authors.

Notes

The authors declare no competing financial interest.

The crystal structures have been deposited in the Protein Database (PDB) under accession numbers 7U6U (ODC G84R/PLP) and 7U6P (ODC G84R). All other data needed to evaluate the conclusions in the paper are presented in the main text.

■ REFERENCES

(1) Mitchell, J. L.; Chen, H. J. Conformational changes in ornithine decarboxylase enable recognition by antizyme. *Biochim. Biophys. Acta* **1990**, *1037*, 115−121.

(2) Coleman, C. S.; Stanley, B. A.; Viswanath, R.; Pegg, A. E. Rapid exchange of subunits of mammalian ornithine decarboxylase. *J. Biol. Chem.* **1994**, *269*, 3155−3158.

(3) Solano, F.; Penafiel, R.; Solano, M. E.; Lozano, J. A. Equilibrium between active and inactive forms of rat liver ornithine decarboxylase mediated by L-ornithine and salts. *FEBS Lett.* **1985**, *190*, 324−328.

(4) Casero, R. A., Jr.; Murray Stewart, T.; Pegg, A. E. Polyamine metabolism and cancer: treatments, challenges and opportunities. *Nat. Rev. Cancer* **2018**, *18*, 681−695.

(5) Matsufuji, S.; Matsufuji, T.; Miyazaki, Y.; Murakami, Y.; Atkins, J. F.; Gesteland, R. F.; Hayashi, S. Autoregulatory frameshifting in decoding mammalian ornithine decarboxylase antizyme. *Cell* **1995**, *80*, 51−60.

(6) Li, X.; Coffino, P. Degradation of ornithine decarboxylase: exposure of the C-terminal target by a polyamine-inducible inhibitory protein. *Mol. Cell. Biol.* **1993**, *13*, 2377−2383.

(7) Pitkanen, L. T.; Heiskala, M.; Andersson, L. C. Expression of a novel human ornithine decarboxylase-like protein in the central nervous system and testes. *Biochem. Biophys. Res. Commun.* **2001**, *287*, 1051−1057.

(8) Chen, H.; MacDonald, A.; Coffino, P. Structural elements of antizymes 1 and 2 are required for proteasomal degradation of ornithine decarboxylase. *J. Biol. Chem.* **2002**, *277*, 45957−45961.

(9) Wu, H. Y.; Chen, S. F.; Hsieh, J. Y.; Chou, F.; Wang, Y. H.; Lin, W. T.; Lee, P. Y.; Yu, Y. J.; Lin, L. Y.; Lin, T. S.; Lin, C. L.; Liu, G. Y.; Tzeng, S. R.; Hung, H. C.; Chan, N. L. Structural basis of antizyme-mediated regulation of polyamine homeostasis. *Proc. Natl. Acad. Sci. U. S. A.* **2015**, *112*, 11229−11234.

(10) Wu, D.; Kaan, H. Y.; Zheng, X.; Tang, X.; He, Y.; Vanessa Tan, Q.; Zhang, N.; Song, H. Structural basis of Ornithine Decarboxylase inactivation and accelerated degradation by polyamine sensor Antizyme1. *Sci. Rep.* **2015**, *5*, 14738.

(11) Prokop, J. W.; Bupp, C. P.; Frisch, A.; Bilinovich, S. M.; Campbell, D. B.; Vogt, D.; Schultz, C. R.; Uhl, K. L.; VanSickle, E.; Rajasekaran, S.; Bachmann, A. S. Emerging Role of ODC1 in Neurodevelopmental Disorders and Brain Development. *Genes* **2021**, *12*, 1−16.

(12) Kabsch, W. Integration, scaling, space-group assignment and post-refinement. *Acta Crystallogr., Sect. D: Biol. Crystallogr.* **2010**, *66*, 133−144.

(13) Zhou, X. E.; Suino-Powell, K.; Schultz, C. R.; Aleiwi, B.; Brunzelle, J. S.; Lamp, J.; Vega, I. E.; Ellsworth, E.; Bachmann, A. S.; Melcher, K. Structural basis of binding and inhibition of ornithine decarboxylase by 1-amino-oxy-3-aminopropane. *Biochem. J.* **2021**, *478*, 4137−4149.

(14) Emsley, P.; Lohkamp, B.; Scott, W. G.; Cowtan, K. Features and development of Coot. *Acta Crystallogr., Sect. D: Biol. Crystallogr.* **2010**, *66*, 486−501.

(15) Adams, P. D.; Afonine, P. V.; Bunkoczi, G.; Chen, V. B.; Davis, I. W.; Echols, N.; Headd, J. J.; Hung, L. W.; Kapral, G. J.; Grosse-Kunstleve, R. W.; McCoy, A. J.; Moriarty, N. W.; Oeffner, R.; Read, R. J.; Richardson, D. C.; Richardson, J. S.; Terwilliger, T. C.; Zwart, P. H. PHENIX: a comprehensive Python-based system for macromolecular structure solution. *Acta Crystallogr., Sect. D: Biol. Crystallogr.* **2010**, *66*, 213−221.

(16) Demeler, B.; Gorbet, G., *Analytical Ultracentrifugation: Instrumentation, Software, and Applications*. Springer: Japan, 2016.

(17) Cao, W.; Demeler, B. Modeling analytical ultracentrifugation experiments with an adaptive space-time finite element solution of the Lamm equation. *Biophys. J.* **2005**, *89*, 1589−1602.

(18) Cao, W.; Demeler, B. Modeling analytical ultracentrifugation experiments with an adaptive space-time finite element solution for multicomponent reacting systems. *Biophys. J.* **2008**, *95*, 54−65.

(19) Brookes, E.; Cao, W.; Demeler, B. A two-dimensional spectrum analysis for sedimentation velocity experiments of mixtures with heterogeneity in molecular weight and shape. *Eur. Biophys. J.* **2010**, *39*, 405−414.

(20) Brookes, E. H.; Demeler, B. In *Parsimonious Regularization using Genetic Algorithms Applied to the Analysis of Analytical Ultracentrifugation Experiments*, GECCO 2007 Proceedings ACM, London, Lipson, H., Ed. Association for Computing Machinery New York NY United States: London, 2007.

(21) Demeler, B.; Brookes, E. Monte Carlo analysis of sedimentation experiments. *Colloid Polym. Sci.* **2008**, *286*, 129−137.

(22) Brookes, E.; Demeler, B. Parallel computational techniques for the analysis of sedimentation velocity experiments in UltraScan. *Colloid Polym. Sci.* **2008**, *286*, 138−148.

(23) Demeler, B.; van Holde, K. E. Sedimentation velocity analysis of highly heterogeneous systems. *Anal. Biochem.* **2004**, *335*, 279−288.

(24) Ghoda, L.; van Daalen Wetters, T.; Macrae, M.; Ascherman, D.; Coffino, P. Prevention of rapid intracellular degradation of ODC by a carboxyl-terminal truncation. *Science* **1989**, *243*, 1493−1495.

(25) Almrud, J. J.; Oliveira, M. A.; Kern, A. D.; Grishin, N. V.; Phillips, M. A.; Hackert, M. L. Crystal structure of human ornithine decarboxylase at 2.1 A resolution: structural insights to antizyme binding. *J. Mol. Biol.* **2000**, *295*, 7−16.

(26) Mullen, P.; Abbott, J. A.; Wellman, T.; Aktar, M.; Fjeld, C.; Demeler, B.; Ebert, A. M.; Francklyn, C. S. Neuropathy-associated histidyl-tRNA synthetase variants attenuate protein synthesis in vitro and disrupt axon outgrowth in developing zebrafish. *FEBS J.* **2021**, *288*, 142−159.

(27) Nagel-Steger, L.; Demeler, B.; Meyer-Zaika, W.; Hochdorffer, K.; Schrader, T.; Willbold, D. Modulation of aggregate size- and shape-distributions of the amyloid-beta peptide by a designed beta-sheet breaker. *Eur. Biophys. J.* **2010**, *39*, 415−422.

(28) Kim, S. K.; Barron, L.; Hinck, C. S.; Petrunak, E. M.; Cano, K. E.; Thangirala, A.; Iskra, B.; Brothers, M.; Vonberg, M.; Leal, B.; Richter, B.; Kodali, R.; Taylor, A. B.; Du, S.; Barnes, C. O.; Sulea, T.; Calero, G.; Hart, P. J.; Hart, M. J.; Demeler, B.; Hinck, A. P. An engineered transforming growth factor beta (TGF-beta) monomer that functions as a dominant negative to block TGF-beta signaling. *J. Biol. Chem.* **2017**, *292*, 7173−7188.

(29) Demeler, B.; Brookes, E.; Wang, R.; Schirf, V.; Kim, C. A. Characterization of reversible associations by sedimentation velocity with UltraScan. *Macromol. Biosci.* **2010**, *10*, 775−782.

(30) Lee, C. Y.; Liu, Y. L.; Lin, C. L.; Liu, G. Y.; Hung, H. C. Functional roles of the dimer-interface residues in human ornithine decarboxylase. *PLoS One* **2014**, *9*, No. e104865.

(31) Pegg, A. E. Regulation of ornithine decarboxylase. *J. Biol. Chem.* **2006**, *281*, 14529−14532.

(32) Rajasekaran, S.; Bupp, C. P.; Leimanis-Laurens, M.; Shukla, A.; Russell, C.; Junewick, J.; Gleason, E.; VanSickle, E. A.; Edgerly, Y.; Wittmann, B. M.; Prokop, J. W.; Bachmann, A. S. Repurposing eflornithine to treat a patient with a rare ODC1 gain-of-function variant disease. *Elife* **2021**, *10*, DOI: 10.7554/eLife.67097.

(33) VanSickle, E. A.; Michael, J.; Bachmann, A. S.; Rajasekaran, S.; Prokop, J. W.; Kuzniecky, R.; Hofstede, F. C.; Steindl, K.; Rauch, A.; Lipson, M. H.; Bupp, C. P. Expanding the phenotype: Four new cases and hope for treatment in Bachmann-Bupp syndrome. *Am. J. Med. Genet., Part A* **2021**, *185*, 3485−3493.

(34) Bupp, C. P.; Schultz, C. R.; Uhl, K. L.; Rajasekaran, S.; Bachmann, A. S. Novel de novo pathogenic variant in the ODC1 gene in a girl with developmental delay, alopecia, and dysmorphic features. *Am. J. Med. Genet., Part A* **2018**, *176*, 2548−2553.